

## Supporting Information

### **Inorganic Nanohybrids Combat Antibiotic-resistant Bacteria Hiding within Human Macrophages**

Martin T. Matter,<sup>1,2</sup> Meagan Doppegieter,<sup>1</sup> Alexander Gogos,<sup>1</sup> Kerda Keevend,<sup>1,2</sup> Qun Ren,<sup>3</sup>  
Inge K. Herrmann<sup>1,2\*</sup>

<sup>1</sup>Laboratory for Particles-Biology Interactions, Department of Materials Meet Life, Swiss Federal Laboratories for Materials Science and Technology (Empa), Lerchenfeldstrasse 5, 9014 St. Gallen, Switzerland.

<sup>2</sup>Nanoparticle Systems Engineering Laboratory, Institute of Process Engineering, Department of Mechanical and Process Engineering, ETH Zurich, Sonneggstrasse 3, 8092 Zurich, Switzerland.

<sup>3</sup>Laboratory for Biointerfaces, Department of Materials Meet Life, Swiss Federal Laboratories for Materials Science and Technology (Empa), Lerchenfeldstrasse 5, 9014 St. Gallen, Switzerland.

[\\*inge.herrmann@empa.ch](mailto:inge.herrmann@empa.ch), [ingeh@ethz.ch](mailto:ingeh@ethz.ch), +41 (0)58 765 71 53

Keywords: bioglass, nanomedicine, antibacterial, ceria, metal oxides

**Table S1:** Dynamic light scattering (DLS) data of the nanoparticles upon suspension in 10% PBS.

	hydrodynamic size (nm)*	zeta potential (mV)
BG	1302 ± 90 (PDI 0.3)	-32 ± 2
Ceria	1089 ± 89 (PDI 0.3)	-35 ± 1
BG/ceria	985 ± 180 (PDI 0.4)	-30 ± 2
Zn2-SrBG/ceria	921 ± 242 (PDI 0.6)	-26 ± 1
BG-Ag0.1%	1574 ± 132 (PDI 0.4)	-25 ± 1
S. aureus	2026 ± 398 <sup>1</sup>	-32 ± 5 <sup>1</sup>

\*limited feasibility of DLS for fractal agglomerates leads to overestimation of size. Formation of agglomerates is especially pronounced in salt-containing media

**Table S2:** Normalized atomic concentration [atomic %] measured by XPS and Ce(III)/Ce(IV) ratio.

Sample	Ce(IV)	Ce(III)	Ce(III)/Ce(IV) ratio
Ceria	81.8	18.2	0.22
BG/ceria	77.3	22.7	0.29
Zn2-SrBG/ceria	80.5	19.5	0.23

**Table S3:** Binding energies (BE) and full width at half maximum (FWHM) of the measured transitions with assignments. Aliphatic C at 285 eV was used for calibration.

Transition	Possible Assignment	BE (eV)	FWHM (eV)
<b>C 1s</b>	C contamination	285.0±0.0	1.7±0.1
<b>O 1s A</b>	metal Oxide	529.6±0.2	1.8±0.2
<b>O 1s B</b>	C=O	531.5±0.3	1.8±0.2
<b>O 1s C</b>	C-O and/or SiOx	533.1±0.6	1.8±0.2
<b>Si 2p</b>	SiOx	102.3±0.3	2.3±0.1
<b>Ce 3d<sub>5/2</sub> v</b>	Ce(IV) Oxide	882.3±0.2	2.0±0.2
<b>Ce 3d<sub>3/2</sub> u</b>		900.9±0.2	2.0±0.2
<b>Ce 3d<sub>5/2</sub> vii</b>		888.8±0.3	4.2±0.7
<b>Ce 3d<sub>3/2</sub> uii</b>		907.4±0.3	4.2±0.7
<b>Ce 3d<sub>5/2</sub> viii</b>		898.3±0.3	2.5±0.3
<b>Ce 3d<sub>3/2</sub> uiii</b>		916.9±0.3	2.5±0.3
<b>Ce 3d<sub>5/2</sub> v0</b>		Ce(III) Oxide	880.2±0.2
<b>Ce 3d<sub>3/2</sub> u0</b>	898.8±0.2		1.1±0.2
<b>Ce 3d<sub>5/2</sub> vi</b>	884.3±0.4		3.4±0.4
<b>Ce 3d<sub>3/2</sub> ui</b>	902.9±0.4		3.4±0.4
<b>Zn2p3</b>	ZnO	1021.8±0.3	2.1±0.0
<b>Na 1s</b>	Sodium compound	1071.7±0.2	2.3±0.1
<b>Ca2p3/2</b>	Ca compound	346.6±0.1	2.1±0.1
<b>Ca2p1/2</b>		350.2±0.2	2.0±0.1

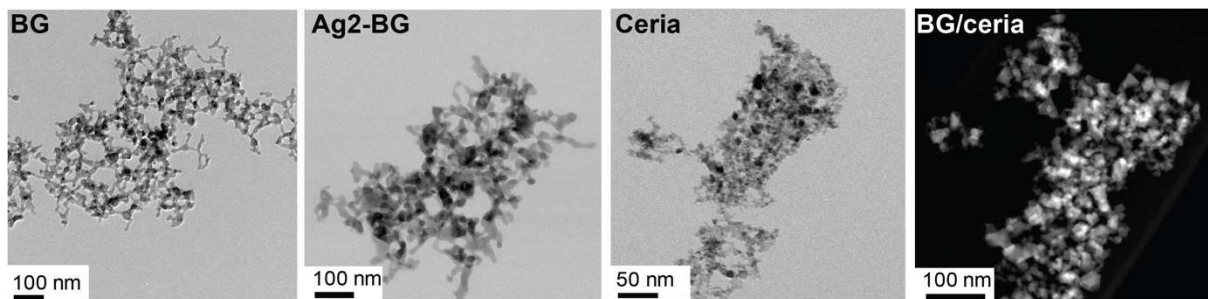


**Figure S1:** Bright-field and dark-field scanning electron micrographs of the as-prepared nanoparticles.

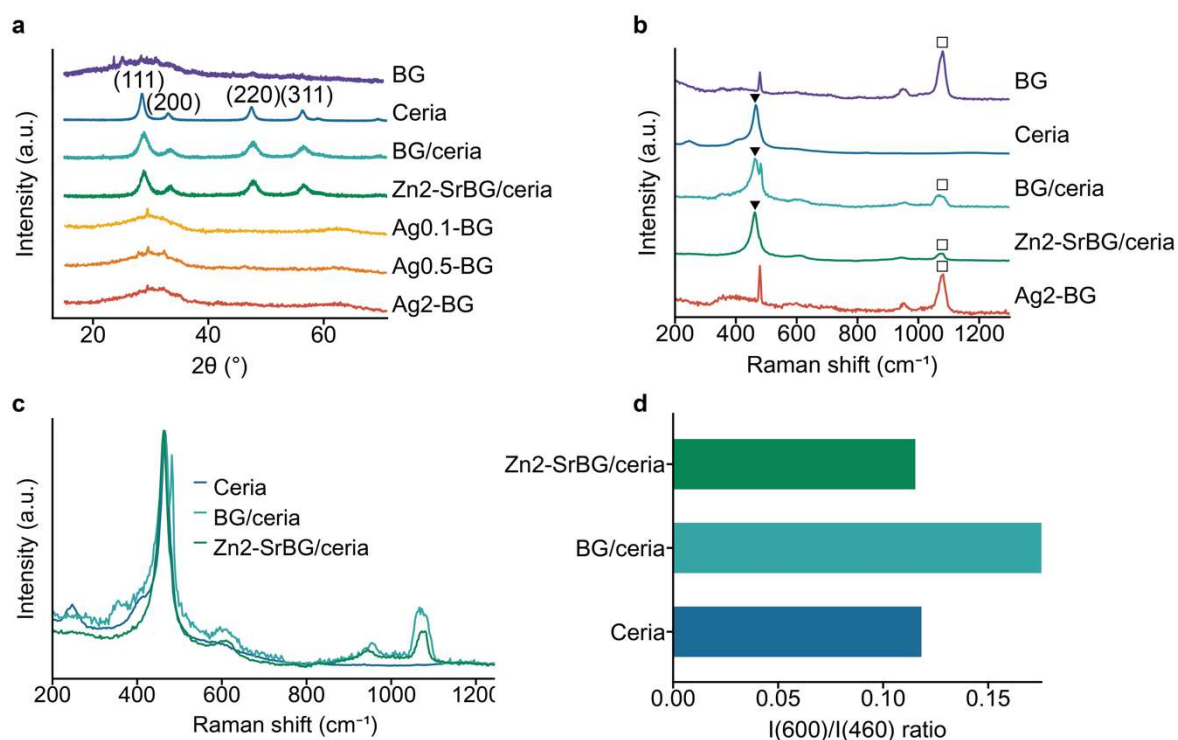


**Figure S2:** a) X-ray powder diffraction patterns. BG and Ag-BGs are highly amorphous without recognizable crystalline peaks. All ceria containing particles have characteristic ceria diffraction patterns (Miller indices shown in parentheses).<sup>2</sup> b) Raman spectra. Characteristic ceria peaks around 465  $\text{cm}^{-1}$  (first-order Raman  $F_{2g}$  mode, Ce-O stretching vibrations<sup>3</sup>, black triangles). Characteristic bioglass peaks<sup>4</sup> around 950  $\text{cm}^{-1}$  and 1050  $\text{cm}^{-1}$  (white rectangles). c) Raman spectra of ceria-containing nanoparticles only. Characteristic ceria peak at 465  $\text{cm}^{-1}$  and different numbers of oxygen defects on the particle surface (at 260  $\text{cm}^{-1}$  and 600  $\text{cm}^{-1}$ ), which correlate to the amount of  $\text{Ce}^{3+}$  on the surface and the particle size.<sup>5</sup> d) Raman intensity ratio of the peak at 600  $\text{cm}^{-1}$  and 460  $\text{cm}^{-1}$  as a qualitative measure of  $\text{Ce}^{3+}$  content.<sup>6,7</sup>

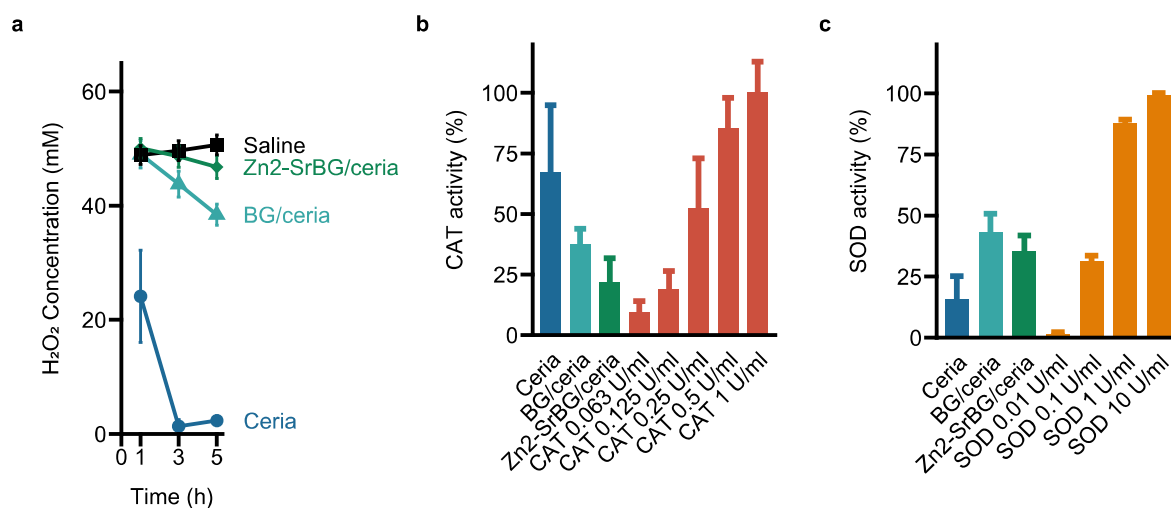


**Figure S3:** a) H<sub>2</sub>O<sub>2</sub> scavenging at 50 mM initial H<sub>2</sub>O<sub>2</sub> concentration for 5 hours. b) Catalase (CAT) mimicry c) Superoxide dismutase (SOD) mimicry. Three independent experiments with four replicates per sample, mean and standard deviation shown.

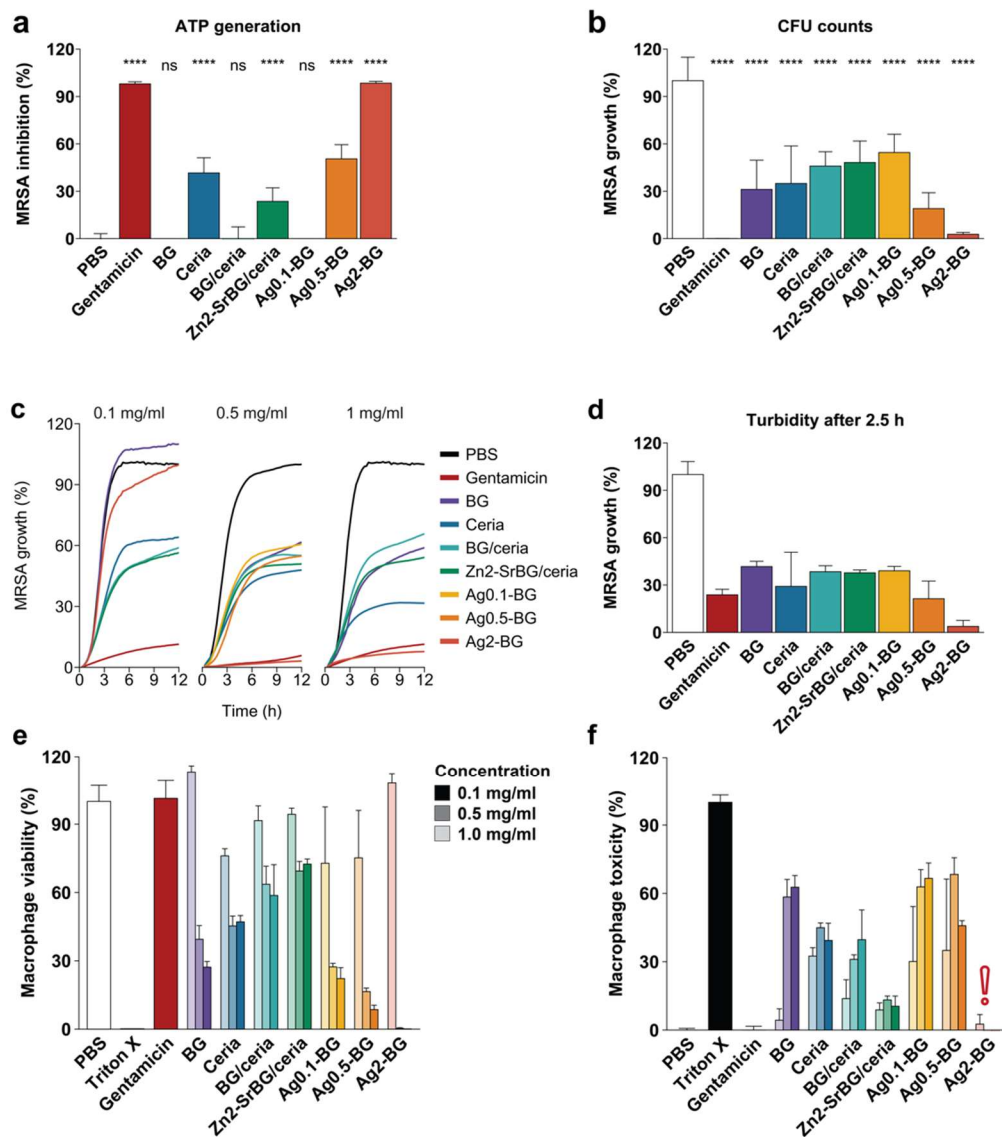


**Figure S4:** (a) Planktonic MRSA inhibition by nanoparticles (0.5 mg/ml) or gentamicin (100  $\mu$ g/ml) based on ATP generation after 2.5 h. Ceria, Zn2-SrBG/ceria, Ag0.5-BG, and Ag2-BG show high bacterial growth inhibition (b) Corresponding planktonic MRSA growth assessed by CFU counting. Control PBS was set as 0 % inhibition and 100 % growth. (c) Growth curves (based on OD<sub>600</sub>) of MRSA treated with various concentrations of nanoparticles or gentamicin (100  $\mu$ g/ml). Bacteria are in their highest growth phase at around t=2.5 h. (d) Turbidity values (based on OD<sub>600</sub>) for the different samples at t=2.5 h and 0.5 mg/ml particle concentration. (e) Macrophage viability assessed by ATP generation following 24 hrs incubation with nanoparticles. (f) Corresponding macrophage toxicity assessed by LDH release which indicates membrane. The red exclamation mark indicates the interference of silver with the LDH assay. Bioglass and silver seem to have an adverse effect on macrophage survival at concentrations >0.5 mg/ml. N=3.

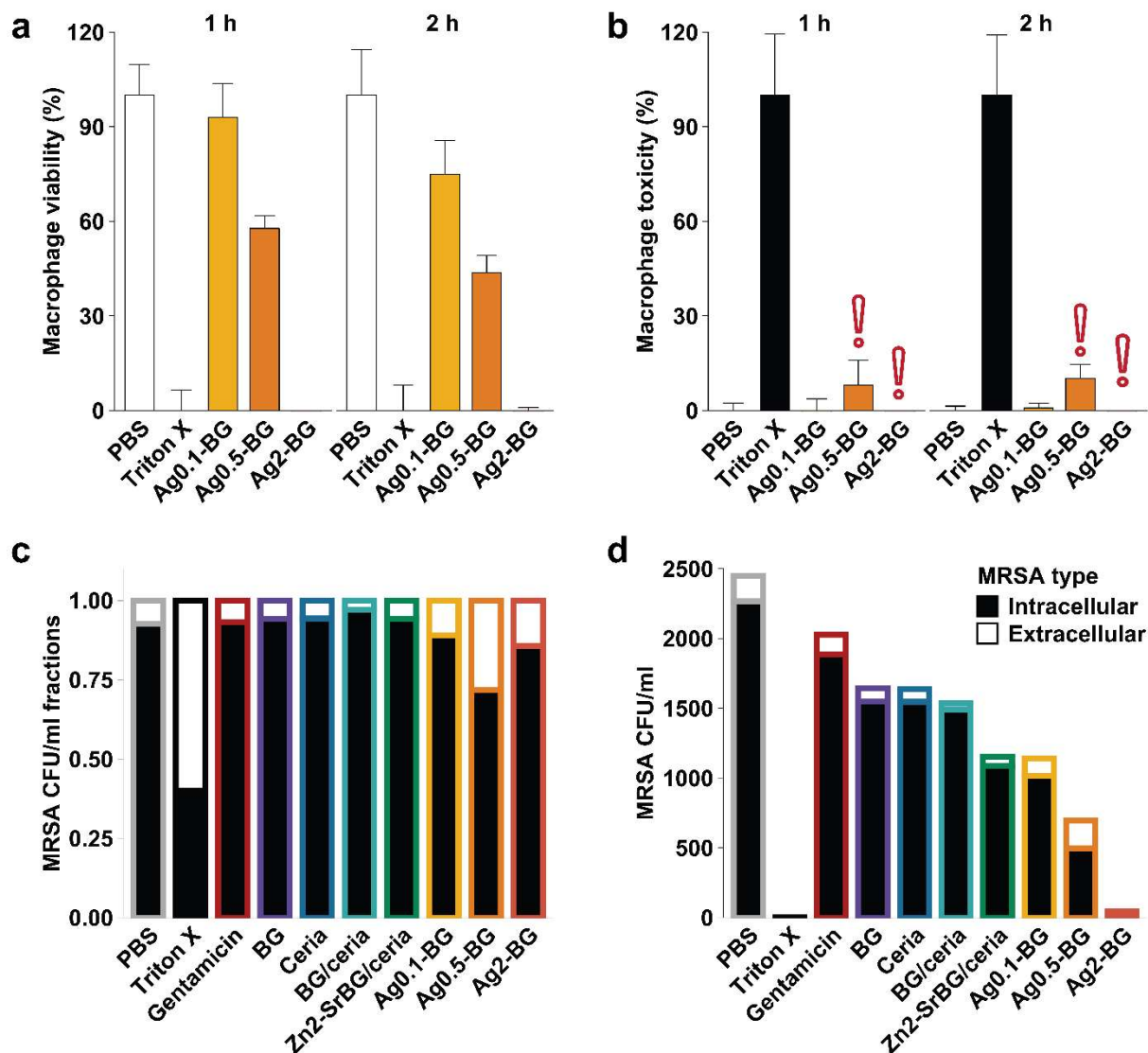


**Figure S5:** Macrophages were incubated with particles and (a) ATP and (b) LDH were measured after 1h and 2h. 0.5mg/ml of Ag0.1-BG, Ag0.5-BG, Ag2-BG or equal volumes of PBS were incubated with RPMI 1640 to test for interference. Macrophage viability assays based on ATP show low cytocompatibility of AgX-BG nanoparticles, which worsens with Ag concentration and contact times. AgX-BG nanoparticles interfere strongly with the cytotoxicity assay based on LDH release as indicated by red exclamation marks. (c) Stacked bar graph on the fraction of intracellular versus extracellular bacteria. Intracellular samples were obtained after macrophage lysis, whereas extracellular MRSA was obtained prior to macrophage lysis. Most bacteria (> 90%) reside intracellularly. Because of cytotoxicity, fewer cells reside in wells treated with Triton X and silver-containing particles. This reduced cell number leads to a higher relative extracellular bacteria count. (d) Stacked bar graph showing absolute CFU/ml values. N=8 for every condition.

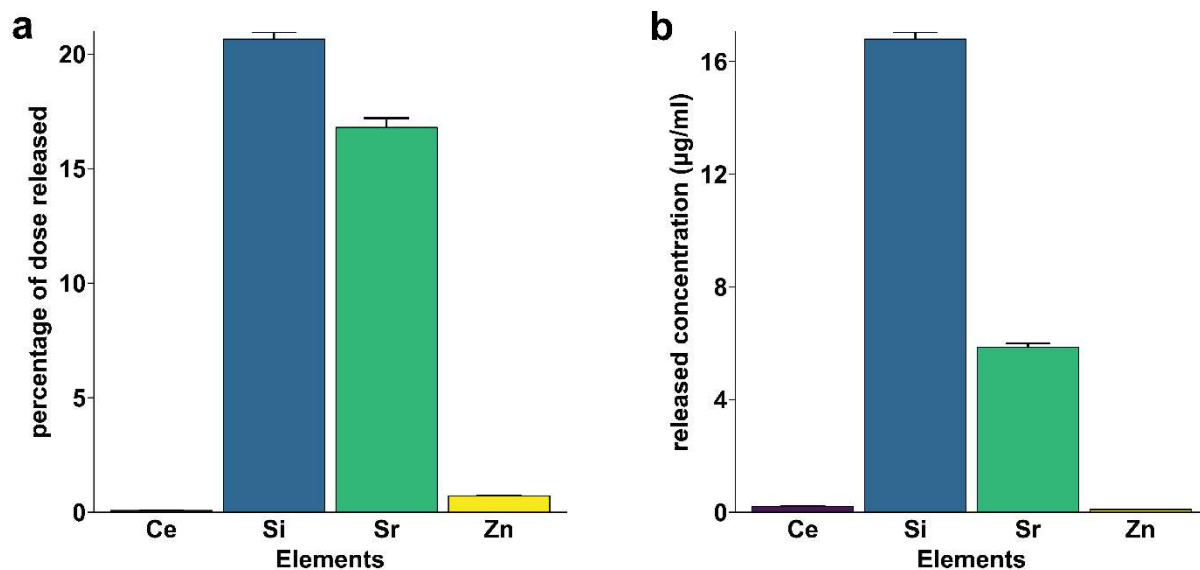


**Figure S6:** Zn<sub>2</sub>-SrBG/ceria nanoparticles were incubated in simulated body fluid for 4 hours. The release of metal ions into the supernatant was measured by ICP-MS. (a) Percentage of the initial element dose, e.g. 20% of the Si contained in Zn<sub>2</sub>-SrBG/ceria was released after 4 hours. (b) The concentration of released elements for the dose (0.5 mg/ml) used for the bacteria experiments. Si and Sr ions are not known to be antibacterial. The measured concentrations of Ce and Zn are orders of magnitude below their reported minimal inhibitory concentrations (MIC, 400 µg/ml<sup>8</sup>-1400 µg/ml<sup>9</sup> for Ce<sup>3+</sup> and 130 µg/ml<sup>10</sup> -1000 µg/ml<sup>11</sup> for Zn<sup>2+</sup>).



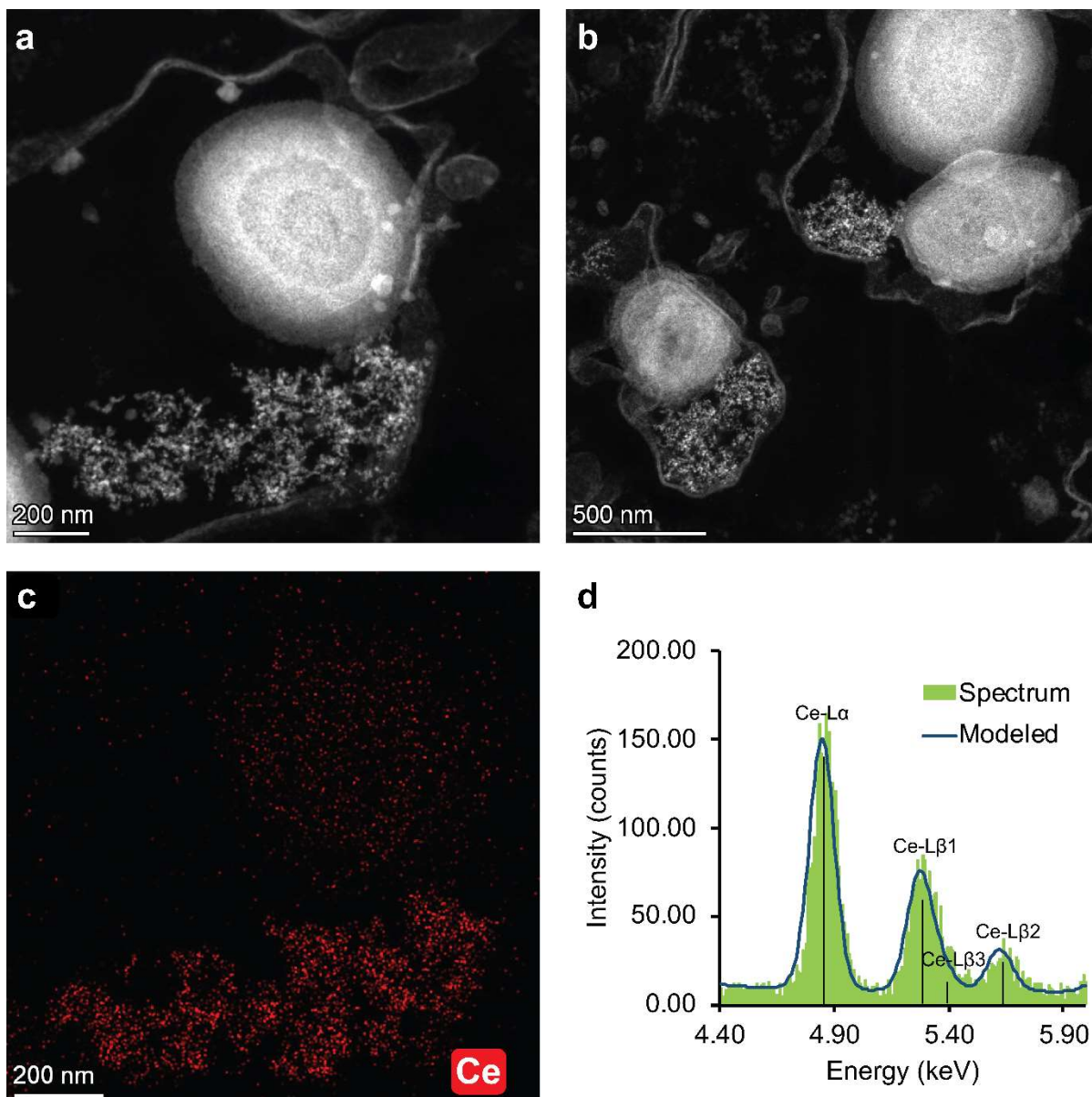


**Figure S7:** (a, b) Dark-field HR-STEM images of MRSA treated with Zn<sub>2</sub>-SrBG/ceria. The lysis of membranes visible as diffuse shells around the bacteria and smaller sizes of the latter. Full lysis upon contact or co-localization with a large number of nanoparticles. The appearance of the lysed intracellular bacteria is comparable to planktonic observations by Ansari et al.<sup>12</sup> (Fig. 5). (c) Ce mapping by EDX (compare a) shows that particle distribution is mostly limited to the particle clusters, but that some found their way through the lysed bacteria. (d) Corresponding EDX spectrum.

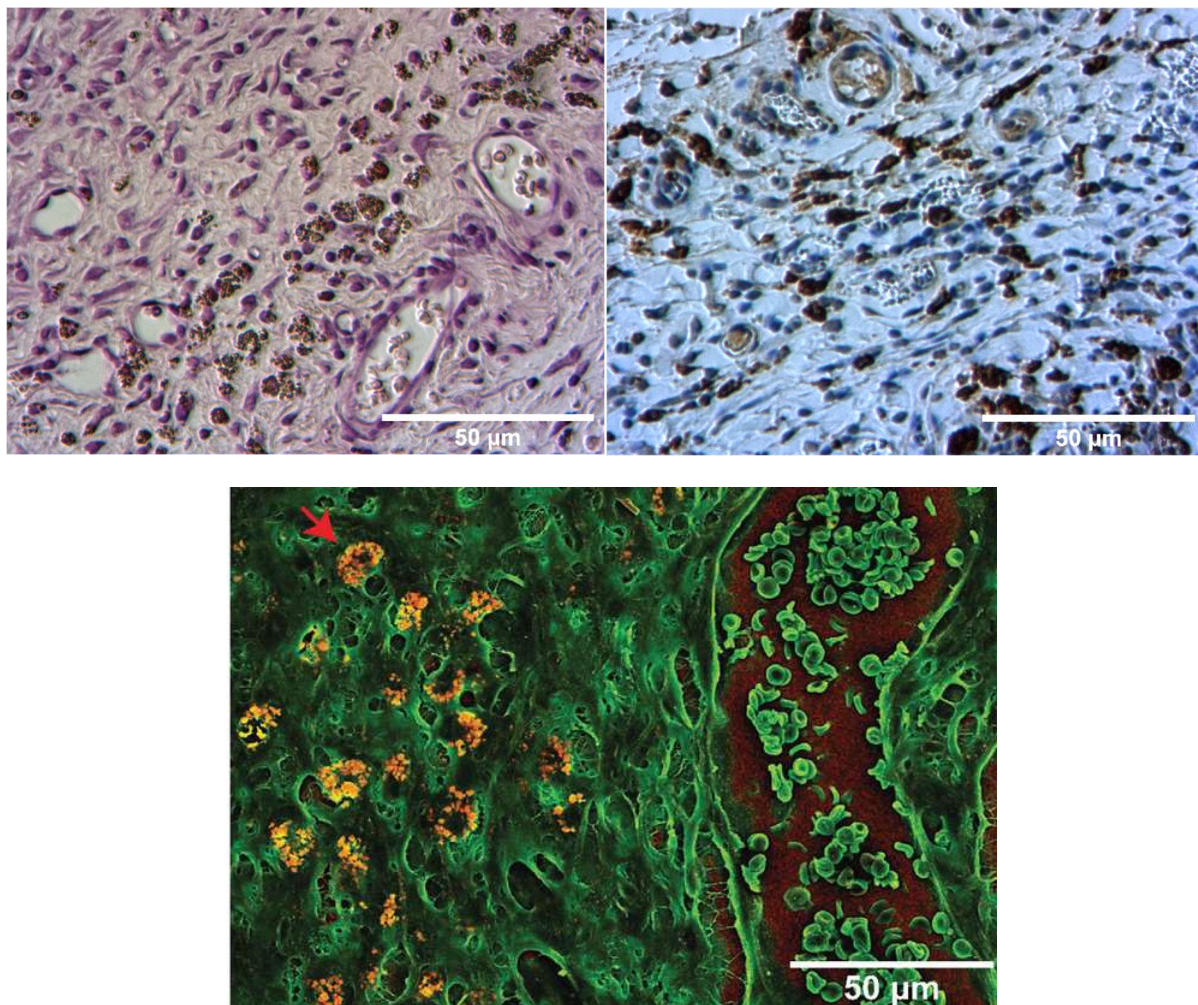


**Figure S8:** Histology sections of rat skin following topical application of BG/ceria nanoparticle suspensions ( $0.1 \text{ mg/cm}^2$ , see Lese et al.<sup>13</sup> for full experimental description). At day 7, accumulation of nanoparticles into cells (H&E, left) that stain positive for CD68 can be observed (right). Density-dependent color scanning electron micrograph of a histological section of the skin flap suggesting accumulation of BG/ceria nanoparticles (in orange) in macrophages and little accumulation in connective tissue (SEM image from Matter et al.<sup>14</sup>)

## References

- 1 Z. Cao, X. Wang, Y. Pang, S. Cheng and J. Liu, *Nat. Commun.*, 2019, **10**, 5783.
- 2 F. Caputo, M. Mameli, A. Sienkiewicz, S. Licocchia, F. Stellacci, L. Ghibelli and E. Traversa, *Sci. Rep.*, 2017, **7**, 4636.
- 3 C. Schilling, A. Hofmann, C. Hess and M. V. Ganduglia-Pirovano, *J. Phys. Chem. C*, 2017, **121**, 20834–20849.
- 4 P. González, J. Serra, S. Liste, S. Chiussi, B. León and M. Pérez-Amor, *J. Non-Cryst. Solids*, 2003, **320**, 92–99.
- 5 R. Jain, A. S. Poyraz, D. P. Gamliel, J. Valla, S. L. Suib and R. Maric, *Appl. Catal. Gen.*, 2015, **507**, 1–13.
- 6 I. Trenque, G. C. Magnano, M. A. Bolzinger, L. Roiban, F. Chaput, I. Pitault, S. Briçon, T. Devers, K. Masenelli-Varlot, M. Bugnet and D. Amans, *Phys. Chem. Chem. Phys.*, 2019, **21**, 5455–5465.
- 7 Y. Xu, F. Wang, X. Liu, Y. Liu, M. Luo, B. Teng, M. Fan and X. Liu, *J. Phys. Chem. C*, 2019, **123**, 18889–18894.
- 8 R. Zhao, Y. Liu, Z. Xie, P. Shen and S. Qu, *Biol. Trace Elem. Res.*, 2002, **86**, 167–175.
- 9 N. M. Zholobak, V. K. Ivanov and A. B. Shcherbakov, in *Nanobiomaterials in Antimicrobial Therapy*, ed. A. M. Grumezescu, William Andrew Publishing, 2016, pp. 419–450.
- 10 M. Čepin, V. Jovanovski, M. Podlogar and Z. C. Orel, *J. Mater. Chem. B*, 2015, **3**, 1059–1067.
- 11 A. Paduraru, C. Ghitulica, R. Trusca, V. A. Surdu, I. A. Neacsu, A. M. Holban, A. C. Birca, F. Iordache and B. S. Vasile, *Materials*, 2019, **12**, 1859.
- 12 M. A. Ansari, H. M. Khan, A. A. Khan, R. Pal and S. S. Cameotra, *J. Nanoparticle Res.*, 2013, **15**, 1970.
- 13 I. Lese, D. A. Graf, C. Tsai, A. Taddeo, M. T. Matter, M. A. Constantinescu, I. K. Herrmann and R. Olariu, *PLOS ONE*, 2018, **13**, e0207802.
- 14 M. T. Matter, J.-H. Li, I. Lese, C. Schreiner, L. Bernard, O. Scholder, J. Hubeli, K. Keevend, E. Tsolaki, E. Bertero, S. Bertazzo, R. Zboray, R. Olariu, M. A. Constantinescu, R. Figi and I. K. Herrmann, *Adv. Sci.*, 2020, **7**, 2000912.